Received: 1 September 2020 | Revised: 11 June 2021 | Accepted: 28 June 2021

DOI: 10.1096/fj.202002039RR

RESEARCH ARTICLE

THE FASEB JOURNAL

Biglycan reduces body weight by regulating food intake in mice and improves glucose metabolism through AMPK/AKT dual pathways in skeletal muscle

InHyeok Chung[1] | Shin Ae Kim[2] | Seolsong Kim[3] | Jung Ok Lee[2] | Clara Yongjoo Park[4] | Juhee Lee[1] | Jun Kang[5] | Jin Young Lee[1] | Ilhyeok Seo[2] | Hye Jeong Lee[2] | Jeong Ah Han[2] | Min Ju Kang[2] | Eunice Lim[6] | Su Jin Kim[2] | Sang Woo Wu[2] | Joo Yeon Oh[2] | Ji Hyung Chung[5] | Eun-Kyoung Kim[3,7] | Hyeon Soo Kim[2] | Min-Jeong Shin[1,8]

[1]Interdisciplinary Program in Precision Public Health, Korea University, Seoul, Republic of Korea

[2]Department of Anatomy, College of Medicine, Korea University, Seoul, Republic of Korea

[3]Department of Brain and Cognitive Sciences, Daegu Gyeongbuk Institute of Science and Technology, Daegu, Republic of Korea

[4]Department of Food and Nutrition, Chonnam National University, Gwangju, Republic of Korea

[5]Department of Biotechnology, CHA University, Gyeonggi-do, Republic of Korea

[6]Department of Molecular & Integrative Physiology, University of Michigan, Ann Arbor, MI, USA

[7]Neurometabolomics Research Center, Daegu Gyeongbuk Institute of Science and Technology, Daegu, Republic of Korea

[8]School of Biosystems and Biomedical Sciences, College of Health Science, Korea University, Seoul, Republic of Korea

Correspondence
Hyeon Soo Kim, Department of Anatomy, College of Medicine, Korea University, Seoul 02841, Republic of Korea.
Email: anatomykim@korea.ac.kr

Min-Jeong Shin, Interdisciplinary Program in Precision Public Health, Korea University, Seoul 02841, Republic of Korea.
Email: mjshin@korea.ac.kr

Funding information
This study was supported by the Basic Science Research Program through the NRF funded by the Ministry of Science and ICT (NRF-2020R1A2C2005580 & NRF-2020R1A2B5B02001468)

Abstract

While biglycan (BGN) is suggested to direct diverse signaling cascades, the effects of soluble BGN as a ligand on metabolic traits have not been studied. Herein, we tested the effects of BGN on obesity in high-fat diet (HFD)-induced obese animals and glucose metabolism, with the underlying mechanism responsible for observed effects in vitro. Our results showed that BGN administration (1 mg/kg body weight, intraperitoneally) significantly prevented HFD-induced obesity, and this was mainly attributed to reduced food intake. Also, intracerebroventricular injection of BGN reduced food intake and body weight. The underlying mechanism includes modulation of neuropeptides gene expression involved in appetite in the hypothalamus in vitro and in vivo. In addition, BGN regulates glucose metabolism as shown by improved glucose tolerance in mice as well as AMPK/AKT dual pathway-driven enhanced glucose uptake and GLUT4 translocation in L6 myoblast cells. In conclusion, our

Abbreviations: AKT, protein kinase B; AMPK, AMP-activated protein kinase; AUC, area under curve; BGN, biglycan; DMEM, Dulbecco's modified Eagle's medium; ECM, extracellular matrix; FBS, fetal bovine serum; GLUT4, glucose transporter type 4; GTT, glucose tolerance test; HFD, high-fat diet; PBS, phosphate-buffered saline; RT-PCR, reverse transcription-polymerase chain reaction.

InHyeok Chung and Shin Ae Kim contributed equally to the study. Eun-Kyoung Kim, Hyeon Soo Kim and Min-Jeong Shin contributed equally to the study.

results suggest BGN as a potential therapeutic target to treat risk factors for metabolic diseases.

KEYWORDS
AKT, AMPK, biglycan, food intake, glucose uptake, obesity

1 | INTRODUCTION

Biglycan (BGN), encoded by the human *bgn* gene located on the X chromosome, is in the class I family of small leucine-rich proteoglycans.[1] BGN was first discovered to comprise part of the extracellular matrix (ECM)[2] and thereby sustain the proper structure and function of tissues. Currently, its soluble form is considered responsible for diverse signaling cascades such as TGF-β and Wnt/β-catenin pathways.[3,4] Binding of BGN to its receptor, TLR2/4, results in the synthesis of pro-inflammatory cytokines such as TNF-α, pro-IL-1β,[5] and cluster purinergic P2X7 receptor-mediated IL-1β maturation,[6] indicating its involvement in inflammatory diseases. In addition, BGN has been suggested to contribute to diverse pathological conditions such as osteoporosis and muscular dystrophy because it stimulates osteoblastic gene transcription[7] and utrophin expression.[8]

Emerging evidence has shown that ECM remodeling is associated with insulin resistance, diabetic nephropathy, and cancers,[9-11] indicating that it displays potential metabolic functions in different tissues.[12] For example, accumulated ECM attenuates vascular insulin delivery in a high-fat diet (HFD),[13] and a reduced hyaluronan level is largely correlated with a robust increase in glycolytic rate.[14] Under stress, BGN spontaneously is released and triggers a danger signal as a part of the immune process.[6] This raises the possibility as to whether BGN is potentially responsible for metabolic alterations in the ECM. In support of this, a possibility has been recently raised that BGN is a myokine which is secreted from skeletal muscle cells during differentiation regulating multiple cellular processes.[15] However, the effects of circulating BGN as a ligand governing metabolic traits require further elucidation.

In this study, we tested the effects of BGN, as a potential candidate for myokine, on metabolic risk factors for type 2 diabetes such as obesity and glucose metabolism in HFD-induced obese animals and the underlying mechanism responsible for the observed effects in vitro. Here, we report that the levels of BGN are increased after exercise in vitro and in vivo, and soluble BGN induces pro-opiomelanocortin (POMC) expression while attenuating agouti-related peptide (Agrp)/neuropeptide Y (NPY) expression in the hypothalamus both in vitro and in vivo. In addition, BGN stimulated glucose uptake in skeletal muscles through GLUT4 translocation, which requires an increase in intracellular Ca^{2+} and a subsequent 5′ AMP-activated protein kinase (AMPK)/AKT-dependent AS160 (T642) phosphorylation. Our results indicate that BGN may be a new strategic target in preventing risk factors for metabolic diseases such as type 2 diabetes mellitus.

2 | MATERIALS AND METHODS

2.1 | Reagents

BGN was purchased from Flarebio (College Park, MD, USA). STO-609 (an inhibitor of calcium/calmodulin-dependent protein kinase kinase, CAMKK) was purchased from SignalChem (St. Louis, MO, USA). 5-aminoimidazole-4-carboxamide ribonucleotide was purchased from Toronto Research Chemical Incorporation (Toronto, ON, Canada). Polyclonal antibodies against phosphorylated AMPKα, acetyl-CoA carboxylase (ACC), phosphorylated ACC, and β-actin were purchased from Millipore (Billerica, MA, USA). AMPKα, AKT, phosphorylated AKT, forkhead box protein O1 (FoxO1), phosphorylated FoxO1, AKT substrate of 160 kDa (AS160), and phosphorylated AS160 were purchased from Cell Signaling Technology (Beverly, MA, USA). GLUT4 was purchased from Abcam (Cambridge, UK). Compound C (an AMPK inhibitor) was provided by Merck (Rahway, NJ, USA). LY-294002 (an AKT inhibitor), Fluo-3 AM, Ionomycin, forskolin, and Verapamil (a calcium channel blocker) were purchased from Sigma (St. Louis, MO, USA). Hybond electrochemiluminescence (ECL) nitrocellulose membranes were obtained from GE Healthcare (Little Chalfont, Buckinghamshire, UK).

2.2 | Cell culture

Rat L6 myoblasts were maintained in DMEM supplemented with 10% fetal bovine serum (FBS), 100 U/mL penicillin, and 100 μg/mL streptomycin at 37°C in 5% CO_2. For myotube differentiation, L6 cells were seeded and grown until confluency. Medium was then supplemented with 2% (v/v) FBS in DMEM. After seven days, the myotube cells were used for further study. Embryonic mouse hypothalamic cell

lines N41 (CLU121) and N43/5 (CLU127) were purchased from Cellutions Biosystems and maintained in DMEM media (Sigma-Aldrich, D5796) supplemented with 10% FBS (Hyclone Laboratories, SH30919.03) and 1% penicillin-streptomycin (Hyclone Laboratories, SV30010) at 37°C and 5% CO_2.

2.3 | Electric pulse stimulation

EPS was applied to myotubes using a C-Pace EP culture pacer (IonOptix, Westwood, MA, USA), which is a multi-channel stimulator designed for chronic stimulation of bulk quantities of cells in culture. The instrument emits bipolar pulses to carbon electrodes of a C-dish. EPS was applied to L6 cells under electrical field of 25 V/cm, with a 5 ms duration and 1 Hz frequency. At the indicated time points, L6 cells were harvested to perform further studies.

2.4 | Western blot analysis

For the in vitro assay, cells were serum-starved for 24 hours and treated with desired time, concentration of BGN. After treatment, cells were lysed in 100 μL RIPA buffer and supernatants were briefly sonicated.

Alternatively, for hypothalamic cell lines, cells were lysed in buffer containing 50 mM Tris-HCl, pH 7.4, 250 mM sucrose, 5 mM sodium pyrophosphate, 1 mM EDTA, 1 mM EGTA, 1% Triton X-100, 0.1 mM benzamidine, 1 mM dithiothreitol, 0.5 mM phenylmethylsulfonyl fluoride, 50 mM sodium fluoride, protease inhibitor cocktail (Millipore, 535140), and phosphatase inhibitor cocktail (Sigma-Aldrich, P5726).

After separating on a 10% SDS-polyacrylamide gel, proteins were transferred onto polyvinylidene difluoride membranes. The membranes were incubated at 4°C overnight with desired primary antibodies and probed by horseradish peroxidase (HRP)-conjugated secondary antibodies. The blots were visualized using an ECL solution (Thermo Fisher Scientific). Quantification was performed by densitometry using Image J software.

2.5 | RNA extraction

RNA extraction was performed by using TRIzol reagent (Invitrogen, 15596018). All steps were accomplished under the manufacturer's suggested protocol. RNA concentration and quality were immediately determined using a Nanodrop 2000 (Thermo Fisher Scientific, Waltham, MA, USA), and aliquots of the total RNA were stored at −80°C until further use.

2.6 | Reverse transcription-polymerase chain reaction

Total RNA (500 ng) was reverse transcribed using AMV Reverse Transcriptase (Promega, Wisconsin, USA). The cDNA was amplified using a GeneAmp PCR System 9700 (Applied Biosystems, Foster City, CA, USA) and then heated to 95°C for 5 minutes to inactivate the reverse transcriptase. PCR was performed using 30 cycles of denaturation at 94°C for 30 seconds, annealing at 55°C for 30 seconds, and amplification at 72°C for 60 seconds, followed by final elongation at 72°C for 10 minutes. The following primers were used for amplification: BGN sense (5′-TGT GGC TAC TCA CCT TGC TG-3′), antisense (5′-ACT TTG CGG ATA CGG TTG TC −3′); β-actin sense (5′-CAG GAG GAG CAA TGA TCT TGA-3′), antisense (5′-ACT ACC TCA TGA AGA TCC TCA-3′). The amplification steps were as follows: 30 cycles of denaturation at 94°C for 30 seconds, annealing at 55°C for 30 seconds, and amplification at 72°C for 60 seconds, followed by final elongation at 72°C for 10 minutes. A 12 μL of PCR product was analyzed by 1.5% agarose gel electrophoresis. The bands obtained were stained with ethidium bromide and visualized under ultraviolet light.

2.7 | Animal and study design

For the exercise model, 10-week-old male ICR mice (24-28 g, Koatech, Gyeonggido, Korea) were used. The mice had ad libitum access to water and food pellets (Cargill Agri Furina, Gyeonggido, Korea), and were housed in a room maintained at 23 ± 2°C with a 12 hours light-dark cycle. After acclimatization for one week, mice were randomly divided into two groups (n = 6/group): control, acute exercise. Acute exercise group mice were subjected to acute forced exercise using a motorized running wheel (20 cm diameter by 5 cm width; Shandong Yiyuan Technology Development Co., Shandong, Binzhou, China). The exercise procedure was performed at a velocity of 10 m/minutes for 60 minutes. When mice failed to run, they were given up to 10 immediate 2.0 mA electric shocks. After a day of exercise, mice were sacrificed, and blood samples were collected for determining serum BGN levels. Detection of serum BGN level was performed using Mouse BGN ELISA kit from Elabscience (Wuhan, Hubei Province, China) according to the manufacturer's instructions. All related protocols were approved by the Institutional Animal Care and Use Committee of Korea University (Korea-2016-0252), and the study was conducted in accordance with the Guide for the Care and Use of Laboratory Animals published by the US National Institutes of Health (NIH).

To investigate the effect of BGN administration on food intake and body weight, wild-type C57BL/6J male mice were

used and obtained from the Central Lab Animal INC (Seoul, Korea) and Koatech Technology Corporation (Pyeongtaek, Korea). Animals were maintained according to the guidelines of the Institutional Animal Care and Use Committee of Korea University (KUIACUC-2018-63). All mice were housed at 18-24°C with a 12-hours light/dark schedule and access to food and water ad libitum. After a week of acclimatization, five-week-old C57BL/6J mice were randomly assigned to normal diet (Normal, n = 10), a HFD (60% fat) (n = 8), and a HFD treated with BGN (HFD + BGN, n = 9) groups. The BGN group was IP injected in every other day for four weeks with BGN (1 mg/kg); Normal and HFD groups received the same volume of phosphate-buffered saline (PBS). For glucose tolerance test, C57BL/6J mice were fasted overnight and injected intraperitoneally (IP) with glucose (diluted in PBS, 1 g/kg). Tail veins were slightly cut to measure blood glucose using a glucometer (Accu-Check, Roche, Germany) at 0, 15, 30, 45, 60, 90, and 120 minutes after glucose injection.

To study the central inhibitory effect of BGN on food intake, five-week-old C57BL/6J mice were anesthetized with a mixture of zoletil (30 mg/kg bodyweight) and rompun (10 mg/kg bodyweight) in NaCl (0.9%) by IP injection. After the loss of reflexes, animals were fixed in a stereotaxic frame (David Kopf Instruments, Tujunga, CA, USA). At the defined positions, small holes were made into the skull using a dental drill. Next, a 26-gauge guide cannula (Plastics One, Roanoke, VA, USA) was implanted into the third ventricle (1.3 mm posterior to the bregma, 5.2 mm below the bregma). The guide cannula was secured to the skull with dental cement (Dentsply, Poly F plus/BONDEX) and covered by a dust cap (Plastics One). After a week of recovery, mice were randomly assigned to 3 groups and administrated with 2 μL of saline (control, n = 5), 0.25 mg/mL BGN (n = 5), and 1 mg/mL BGN (n = 5), respectively. Injection was performed on the third ventricle 1 hour prior to the beginning of the dark cycle. Food intake and body weight change were measured at 3, 6, 12, and 24 hours after BGN administration. During the assay, all mice were allowed to access to food (normal diet) and water ad libitum. All related protocols followed National Institutes of Health guidelines and were approved by the Institutional Animal Care and Use Committees at DGIST Laboratory Animal Resource Center (DGIST-IACUC-17112801-00).

2.8 | Reverse transcription quantitative PCR

Obtained RNA (1 μg) was reverse-transcribed, and qPCR was performed using SYBR-Green and quantified by QuantStudio 6 flex (Thermo Fisher Scientific) and the CFX 96 Real-Time system (Bio-Rad, Hercules, CA, USA). All reactions were performed by the following conditions: 40 cycles of denaturation at 94°C for 60 seconds, annealing at 55°C for 30 seconds, and amplification at 72°C for 60 seconds, followed by final elongation at 72°C for 10 minutes. The expression level of each gene was normalized to that of Gapdh as an endogenous control. Primers used were as follows: Agrp sense (5′-CTGCAGACCGAGCAGAAGA-3′), antisense (5′-TGCGACTACAGAGGTTCGTG-3′); NPY sense (5′-CAGAAAACGCCCCC-AGAA-3′), antisense (5′-AAAAGTCGGGAGAACAAGTTTCATT-3′); POMC sense (5′-GAACAGCCCCTGACTGAAAA-3′), antisense (5′-ACGTTGGGGTACACCTTCA-C-3′); Gapdh sense (5′-ATCACTGCCACCCAGAAGAC-3′), antisense (5′-ACACATT-GGGGGTAGGAACA-3′).

2.9 | Uptake of 2-deoxy-D(H^3)-glucose

Glucose uptake was determined by detecting the intracellular level of 2-deoxy-D(H^3)-glucose (2-DG) in differentiated L6 myotubes. First, cells were starved in serum-free DMEM for 3 hours. The cells were then stimulated with BGN and incubated in Krebs–Ringer bicarbonate (KRB) buffer (20 mM HEPES [pH 7.4], 130 mM NaCl, 1.4 mM KCl, 1 mM $CaCl_2$, 1.2 mM $MgSO_4$, and 1.2 mM KH_2PO_4) buffer containing 0.5 μCi 2-DG at 37°C for 15 minutes. Cells were lysed in 0.5 N NaOH, and lysates were mixed with 3.5 mL of scintillation cocktail. Radioactivity was measured by scintillation counting.

2.10 | Myc-GLUT4 translocation assay

Cell surface expression of Myc-GLUT4 was quantified by performing an antibody-coupled colorimetric absorbance assay. L6 myotubes stably expressing Myc-GLUT4 were stimulated with BGN and simultaneously incubated with polyclonal anti-Myc antibody (1:1000) for 60 minutes. Cells were fixed with 4% paraformaldehyde in PBS for 10 minutes and incubated with HRP-conjugated goat anti-rabbit antibody (1:1000) for 1 hour. After washing with PBS six times, cells were incubated in 1 mL *o*-phenylenediamine (0.4 mg/mL) for 30 minutes. The absorbance of the supernatant was measured at 492 nm.

2.11 | Immunofluorescence staining

Cells were fixed with 4% paraformaldehyde and permeabilized with 0.2% Triton-X 100. After incubation with 0.2% bovine serum albumin for 30 minutes, cells were incubated with an anti-GLUT4 antibody at a 1:500 dilution for 60 minutes and probed with a Cy3-labeled secondary antibody (Molecular Probes, Eugene, OR, USA). For counterstaining

the nuclei, samples were incubated with 0.5 μg/mL DAPI (4′,6-diamidino-2-phenylindole) for 10 minutes. Cells were visualized under confocal microscopy (Zeiss LSM 510 Meta; Zeiss, Oberkochen, Germany).

2.12 | Intracellular Ca^{2+} measurement

To determine intracellular Ca^{2+} concentrations, L6 cells were incubated with 5 mM Fluo-3 AM for 45 minutes at 37°C in a 5% CO_2 incubator. After washing briefly with PBS, the cells were observed by confocal microscopy (Zeiss LSM 510 Meta). The wavelength for excitation was 488 nm and emission 515 nm.

2.13 | siRNA transfection

L6 cells were transfected with siRNAs targeting AMPKα2 (L-100623, Dharmacon, GE Healthcare) and AKT2 (L-091136, Dharmacon, GE Healthcare) according to the manufacturer's protocol. In brief, siRNAs and Lipofectamine 2000 were diluted in reduced serum medium (Opti-MEM; Invitrogen, Carlsbad, CA USA) and mixed. The mixture was incubated for 30 minutes at room temperature and then added dropwise until the final siRNA concentration reached 100 nM. The medium was replaced with fresh complete medium after 6 hours of transfection.

2.14 | Statistical analyses

The results are presented as means ± standard error of the mean (SEM), and the differences among the experimental groups were analyzed using the Student's *t*-test (for the in vitro experiments) and one-way analysis of variance (ANOVA) with Fisher's least significant difference post-hoc test (for the animal experiments). To compare means among the three groups for body weight change and glucose tolerance test in mice, two-way ANOVA with repeated measures was performed with Bonferroni post-hoc test was performed. Differences with values of $P < .05$ were considered statistically significant.

3 | RESULTS

3.1 | BGN is induced with exercise and present in mouse serum

The ability of skeletal muscle to effect on mechanistic properties by releasing extracellular components during the exercise is already well-known. However, when it is transited to soluble form as cleaved from extracellular matrix (ECM), BGN acts to initiate diverse signaling cascades unlike other ECM components. This allowed us to investigate the relevant physiological effects of increase in BGN secretion under exercise. We, then first tested whether exercise actually contributes to skeletal muscle cells to secret BGN into blood. Under electrical pulse stimulation system (EPS), in vitro exercise model, L6 myotubes appeared to elevate AMPK phosphorylation (Figure 1A) which is occurred during exercise.[16] In the same condition, we observed the increase in mRNA level of *bgn* in early response from 1 to 6 hours (Figure 1B). This was further confirmed by introducing combination of ionomycin and forskolin to L6 myotubes regarding such compounds are reported to mimic exercise condition.[17] Ionomycin and forskolin cause an increase in AMPK phosphorylation for 6 hours (Figure 1C) and *bgn* mRNA expression which peaked at 0.5 hours and retained for 3 hours (Figure 1D), compared to control. Consistently, we observed the similar results in primary cultured myoblasts (see Figure S1A,B). Upon this, we assessed the level of BGN mRNA in skeletal muscle by using exercised mice model and there was elevation of mRNA expression (See Figure S2A). To validate the direct exercise-BGN secretion mechanism, we utilized animal study using ICR mice acutely exercised and observed a significant increase in serum BGN levels (Figure 1E). Thus, exercise derives increased secretion of BGN on skeletal muscle.

3.2 | BGN prevents weight gain in HFD-induced obese mice by reducing food intake

Next, we tested whether BGN contributes to mediate metabolic disturbances by injecting soluble BGN into HFD-induced obesity mice model. As shown in Figure 2A, after four weeks of obesity induction and five additional weeks, significant differences in body weight gains arose between the HFD and HFD + BGN (1 mg/kg body weight) groups. Final body weights were significantly lower in the HFD + BGN group than that in HFD group (Figure 2B). In addition, the HFD + BGN group consumed significantly less food than the HFD group (Figure 2C,D). While differences in total fat weight (calculated as the sum of epididymal fat and subcutaneous fat) between the HFD and HFD + BGN groups were not significant (Figure 2E), interestingly, the average amount of quadriceps muscle was significantly higher in the HFD + BGN group compared with that of the HFD group (Figure 2F).

3.3 | BGN regulates hypothalamic neuropeptide gene expression

To elucidate the mechanism by which BGN administration reduces food intake, we first hypothesized that BGN modulates

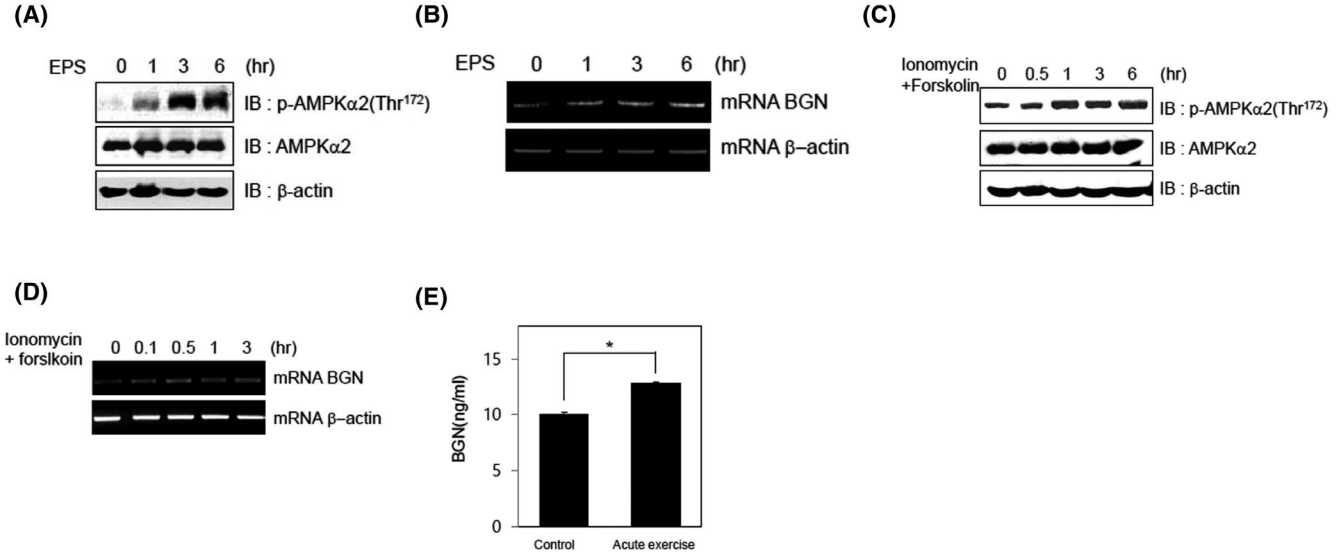

FIGURE 1 Increase in AMPK activity and circulating BGN during exercise. A-D, L6 myoblasts were differentiated for seven days and then stimulated with an electrical pulse stimulation system (EPS) for 6 hours while (C, D) co-stimulation of ionomycin (0.5 μM) and forskolin (1 μM) served as control. A and C, Cells were subjected to western blotting against p-AMPKα2, AMPKα2, and β-actin. B and D, Total mRNA was extracted from cells, and reverse transcription-polymerase chain reaction was performed using BGN. β-actin mRNA levels were used for normalization. E, Serum BGN levels in acutely exercised mice and not exercised control mice were measured. $*P < .05$. Data are expressed as mean ± SEM

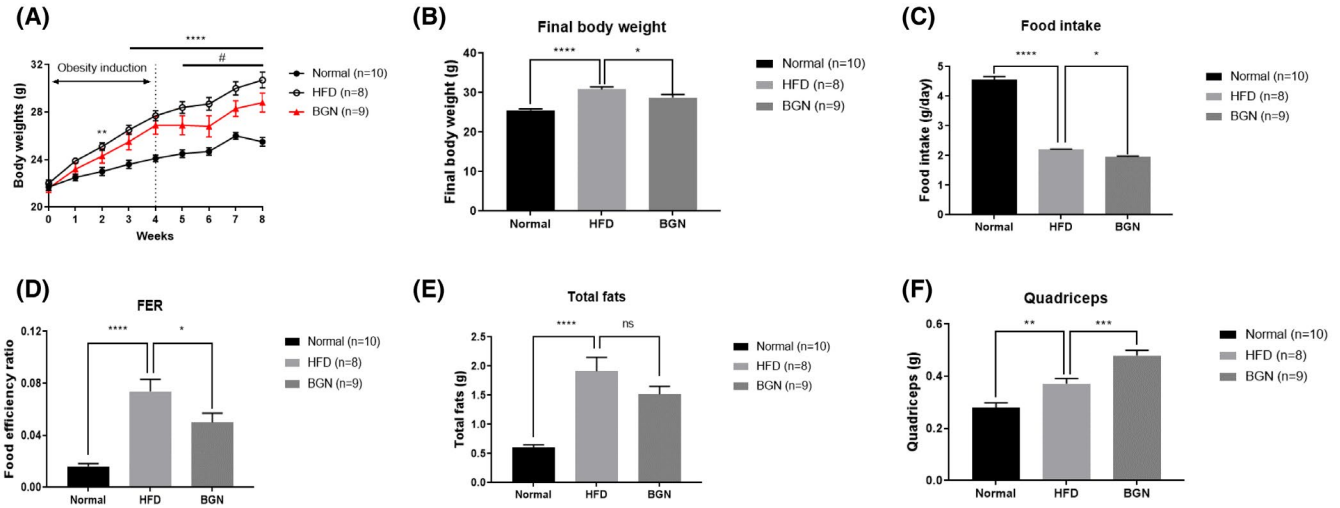

FIGURE 2 BGN reduces food intake and prevents weight gain in high-fat diet-induced obese animals. A-F, C57BL/6J mice were fed a normal diet (ND; n = 10) or a high-fat diet (HFD) and injected intraperitoneally (IP) with PBS (n = 8) or BGN (n = 9). A, Body weights of mice were measured daily and (B) final body weights, (C) average daily food intake (g/day), (D) food efficiency ratio (FER, food intake/weight gain), (E) total fat mass, and (F) muscle (quadriceps femoris) mass were determined at the day of sacrifice. $*P < .05$, $**P < .01$, $***P < .001$, $****P < .0001$. $^{\#}P < .05$, compared with HFD control. ns; not significant. All data are expressed as mean ± standard error of the mean (SEM)

the gene expression of neuropeptides involved in appetite regulation in the hypothalamus. The mouse embryonic hypothalamic cell lines N41 (expressing Agrp/NPY) and N43/5 (expressing POMC) were used to measure orexigenic and anorexigenic neuropeptides expression, respectively. Upon BGN treatment in N41 cells for 1 hour, mRNA expression of Agrp and NPY was significantly decreased (Figure 3A,B). By contrast, significantly elevated POMC expression was observed in N43/5 cells at 12 hours after BGN treatment (100 ng/mL) (Figure 3C). These results suggest that BGN reduces the appetite through hypothalamic regulation by up-regulating the expression of anorexigenic neuropeptides and downregulating the expression of orexigenic neuropeptides.

We next investigated whether intracerebroventricular (ICV) injection of BGN influences food intake to test whether the effect of BGN on appetite regulation is

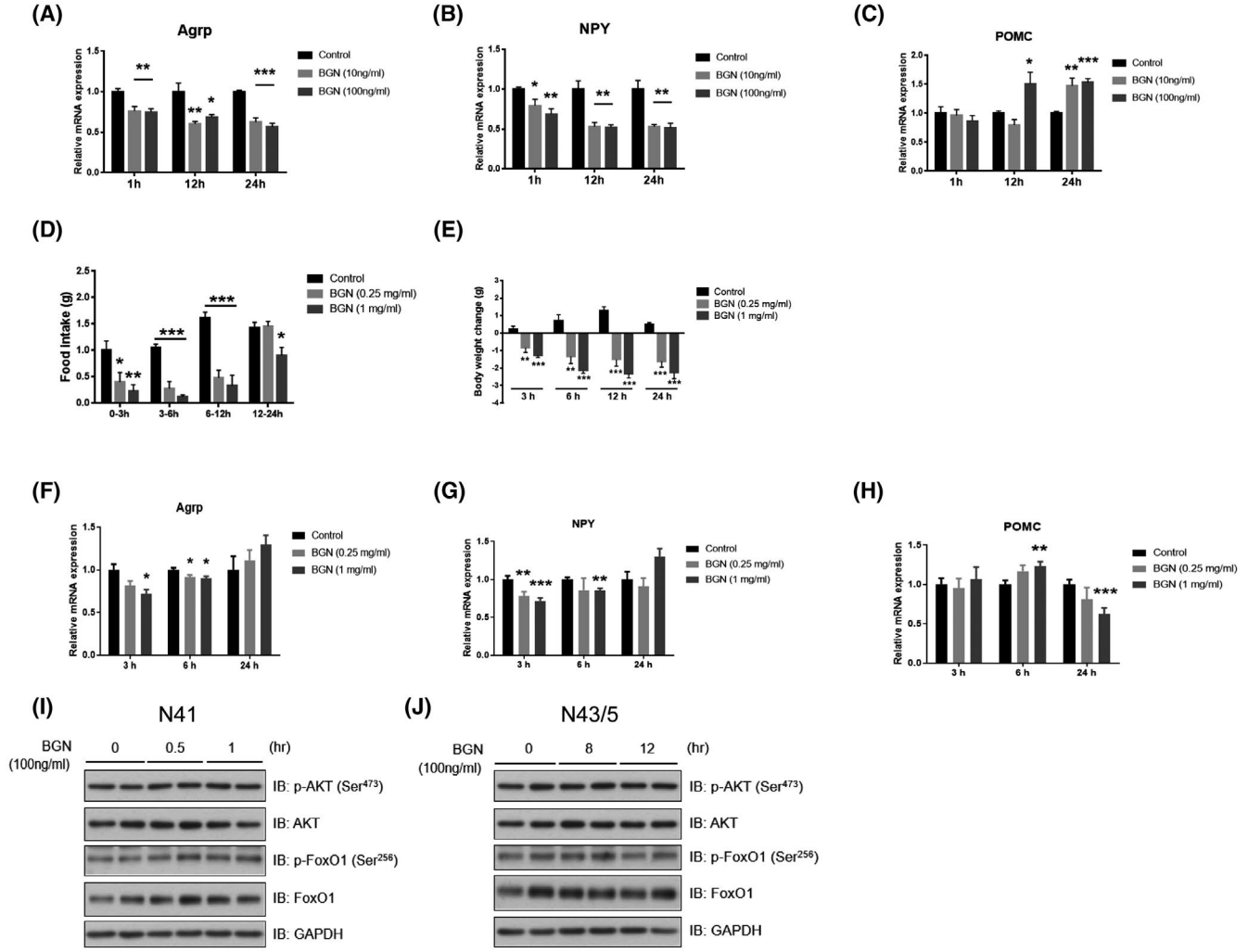

FIGURE 3 BGN modulates expression of genes involved in appetite in vitro and in vivo while not affecting AKT/FoxO signal. A-C, Real-time reverse-transcriptase (RT)-PCR analysis in N41 and N43/5 hypothalamus cell lines. Cells were treated with BGN as indicated and were examined. Bar graph shows the relative mRNA expression against (A) Agrp, (B) NPY, and (C) POMC. D-H, C57BL/6J mice were received intracerebroventricular (ICV) injections of BGN as indicated for dose and time. D, Food intake and (E) body weight change were measured before and after BGN administration. F-H, Relative gene expression changes from mouse hypothalamus tissues. Bar graph shows the relative mRNA expression against (F) Agrp, (G) NPY, and (H) POMC. $*P < .05$, $**P < .01$, $***P < .001$. A and B, BGN (100 ng/mL) was treated in hypothalamic cell line (A) N41 and (B) N43/5 for indicated time. Lysates were used for western blot against P-AKT, AKT, P-FoxO1, FoxO1, and GAPDH. A-C, Data are expressed as mean ± SEM (n = 3)

biologically relevant. Consistent with the observed effect in vitro, mice injected with BGN consumed significantly less food than mice injected with saline until 24 hours after injection (Figure 3D). Body weight was decreased in a time- and dose-dependent manner (Figure 3E). Notably, hypothalamic expression of Agrp/NPY in mice was reduced at all time points until 6 hours, when POMC expression was increased. However, at 24 hours, expression of these neuropeptides was reversed, perhaps as a rebound effect to maintain homeostasis (Figure 3F-H). To determine which molecular pathway is responsible for BGN-mediated reduction of food intake, we targeted the AKT and its downstream FoxO1 which is a well-known regulatory pathway for hypothalamic neuropeptide expression.[18] Unexpectedly, BGN treatment did not affect the phosphorylation of AKT and FoxO1 in N41 and N43/5 cells (Figure 3I,J).

3.4 | Effects of BGN on glucose metabolism in HFD-induced obese animals and skeletal muscle cells

Because POMC neurons are glucose-excited neurons and responsible for glucose control,[19] an increase in POMC expression by BGN treatment raises the question of whether BGN also regulates glucose metabolism. We performed an intraperitoneal glucose tolerance test to determine the peripheral effects of BGN on glucose metabolism in HFD-induced

obese mice. Following IP injection of 1 mg/kg BGN, the HFD + BGN group demonstrated significant improvement in glucose metabolism, as measured by glucose area under curve, than that of the HFD mice (Figure 4A,B).

Our observation of increased muscle mass upon BGN treatment potentiates an uncharacterized effect of soluble BGN on muscle tissue under physiological condition. As tested in L6 myoblast cells, BGN markedly increased uptake of various concentrations of glucose compared with controls (Figure 4C). Glucose uptake peaked at 0.3 μg/mL BGN, and BGN-induced glucose uptake was sustained until 18 hours post-stimulation (Figure 4D). Additionally, we observed that over 0.1 μg/mL of BGN had a greater impact on glucose uptake than insulin alone (positive control). Because glucose enters into muscle cells facilitated through the GLUT4 transporter, we then tested whether BGN stimulation promotes the translocation of the GLUT4 protein into the cell membrane. As expected, BGN administration resulted in following significant increase of translocation of GLUT4 (Figure 4E) and this was visually confirmed by using confocal microscopy (Figure 4F). Together, these results indicate that BGN improves glucose homeostasis by enhancing GLUT4 translocation and glucose uptake.

3.5 | BGN stimulates AMPK activation and promotes Ca^{2+}-dependent glucose uptake in skeletal muscle

Expression of BGN has been reported to increase in the skeletal muscle of Duchenne muscular dystrophy patients and binds to the dystrophin-glycoprotein (DGC) complex, suggesting BGN's role in muscle regeneration and integrity.[20] The function of soluble BGN in the skeletal muscle, however, is currently unknown. To elucidate the underlying mechanism by which BGN regulates glucose uptake, we tested whether BGN influences the AMPK intracellular pathway in skeletal muscles. It has been widely known that AMPK sense the glucose molecule and promote glucose uptake during exercise.[21] Our results showed that BGN promoted phosphorylation of AMPK and its downstream effector ACC in a dose-dependent manner (Figure 5A), which was also confirmed in primary cultured myoblast cells (see Figure S1C). Notably, AMPK activation peaked at 0.5 hour and slowly declined, implying BGN's early effects in cell systems (Figure 5B) and this was significantly blocked by compound C (an AMPK inhibitor) (Figure 5C). Given that AMPK promotes glucose uptake with CAMKK under stimulation with diverse hormones,[22] we investigated

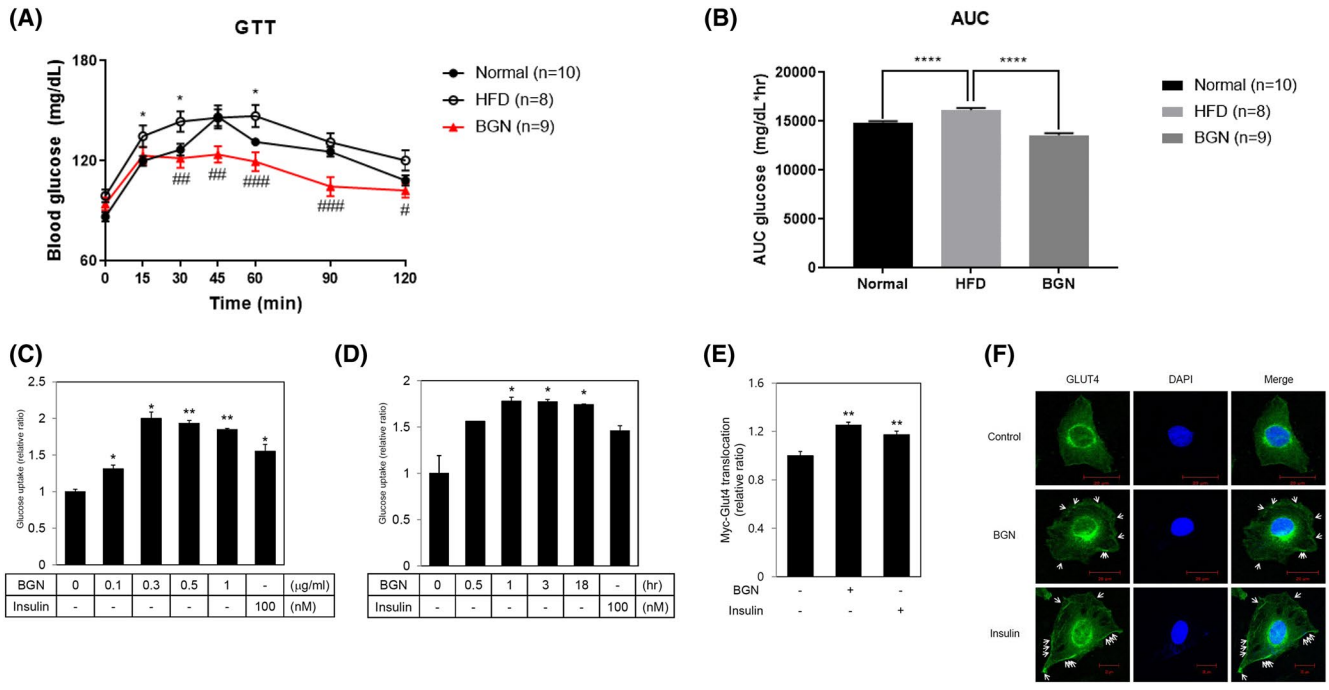

FIGURE 4 BGN improves glucose metabolism in high-fat diet-induced obese animals and L6 cells. A-B, Effect of BGN on glucose metabolism was evaluated in high-fat diet (HFD)-induced obese mice. A, Glucose tolerance test (GTT) was performed on normal diet (ND; n = 10), HFD (n = 8), and HFD + BGN (n = 9) mice and (B) quantified as the area under curve (AUC). C-E, L6 cells were differentiated to myotubes for seven days to determine whether BGN affects glucose uptake in skeletal muscle. C and D, Relative glucose uptake value in myotubes treated with (C) BGN (0-1 μg/mL) for 1 hour or (D) 18 hours with a fixed dose (0.3 μg/mL). E, Relative value of surface myc-GLUT4 in myotubes treated with BGN (0.3 μg/mL). F, Representative confocal images of L6 myoblast cells treated with BGN (0.3 μg/mL). *Green*; GLUT4, *Blue*; DAPI (nuclei). Insulin was introduced as a positive control. A and B, $^{*}P < .05$, $^{****}P < .0001$. $^{\#}P < .05$, $^{\#\#}P < .01$, $^{\#\#\#}P < .001$, compared with HFD control. Data are expressed as mean ± standard error of the mean (SEM). C-E, $^{*}P < .05$, $^{**}P < .01$. Data are expressed as mean ± SEM (n = 3)

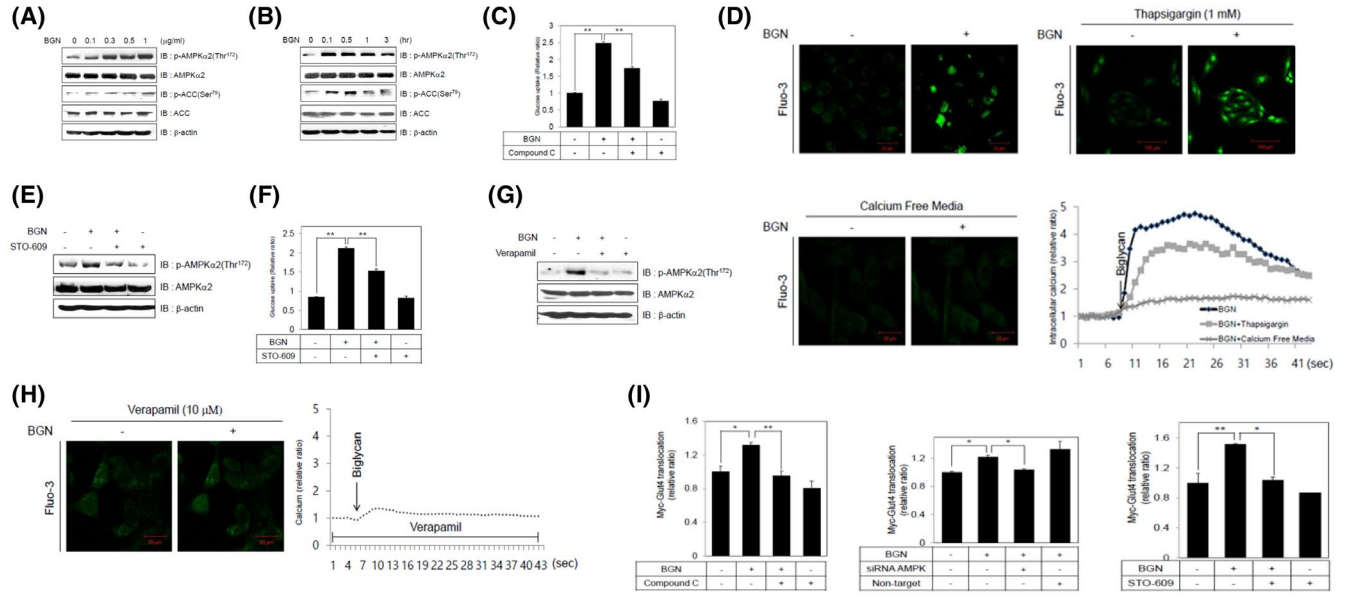

FIGURE 5 BGN stimulates glucose uptake through AMPK in a Ca^{2+}–dependent manner in L6 myoblast cells. L6 rat myoblast cells were incubated with (A) BGN (0-1 μg/mL) for 1 hour or (B) 3 hours with a fixed dose of BGN (0.3 μg/mL). Lysates were used for western blot against AMPKα2, p-AMPKα2, ACC, p-ACC, and β-actin. C, F, I, L6 cells were differentiated to myotubes for seven days to determine whether BGN affects glucose uptake or myc-GLUT4 translocation in skeletal muscle. C, Myotubes incubated with BGN (0.3 μg/mL) for 1 hour in the presence of the compound C (AMPK inhibitor, 30 μM) were then assayed for glucose uptake. For intracellular calcium detection, (D) L6 cells were pre-incubated in Fluo-3AM (5 μM) for 45 minutes and then treated with BGN (0.3 μg/mL), left upper panel. To compare, L6 cells were cultured in only calcium-free medium (left lower panel) or pre-incubated with thapsigargin (intracellular calcium chelator, 1 mM) for 3 hours (right upper panel). Images were analyzed for fluorescence intensity and presented as intracellular calcium levels (right lower panel). E and F, The role of CAMKK was assessed by incubating STO-609 (CAMKK inhibitor, 5 μM) for 1 hour, following 1 hour stimulation of BGN (0.3 μg/mL) in (E) L6 cells and (F) myotubes. Levels of activated AMPK and glucose uptake are shown, respectively. G, L6 cells were pre-treated for 1 hour with verapamil (calcium channel blocker, 10 μM) and incubated with 0.3 μg/mL BGN for an additional 1 hour. Obtained cell lysates were analyzed by western blotting. H, L6 cells were pre-incubated with verapamil (10 μM) for 30 minutes and treated with Fluo-3AM (5 μM) and BGN (0.3 μg/mL). Obtained images are shown (left panel) and were analyzed for fluorescence intensity (right panel). I, To compare surface myc-GLUT4 levels, myotubes were treated with BGN (0.3 μg/mL) in the presence of 30 μM compound C (left panel) or 5 μM STO-609 (right panel). Myotubes lacking AMPK were treated with BGN (0.3 μg/mL), middle panel. Surface myc-GLUT4 level was quantified using an antibody-coupled colorimetric absorbance assay. Non-target antibody was used as a negative control. $*P < .05$, $**P < .01$. All data are expressed as mean ± SEM (n = 3)

the role of Ca^{2+} in regulating the function of BGN. As shown in Figure 5D, BGN increases fluorescence intensity, indicating that BGN increases intracellular Ca^{2+} levels. The increase of fluorescence intensity is not affected by thapsigargin, an inhibitor of sarco/endoplasmic reticulum Ca^{2+} ATPase (SERCA), implying that this is mediated by cellular uptake of Ca^{2+}. Increases in intracellular Ca^{2+} levels by BGN treatment were also confirmed in primary cultured myoblast cells (see Figure S1D). In response to Ca^{2+} uptake, CAMPKK combines with AMPK, and this was confirmed using STO-609, a CAMKK inhibitor (Figure 5E,F). Interestingly, inhibition of CAMKK significantly abrogates BGN-induced glucose uptake, implicating Ca^{2+} as a key factor in this phenomenon. Importantly, we also observed the ineffectiveness of BGN in the presence of verapamil, a calcium channel antagonist (Figure 5G,H). These results collectively suggest that the action of BGN is mediated by the AMPK-CAMKK complex and is initiated with cellular Ca^{2+} uptake. This was further confirmed as compound C, AMPK-specific siRNA, and STO-609 successfully blocked BGN-mediated GLUT4 translocation (Figure 5I).

3.6 | BGN stimulates glucose uptake via AKT activation in skeletal muscles

Because AMPK-mediated glucose uptake is reported to be insulin-independent, we next investigated whether AKT, a crucial regulatory factor of insulin signal on glucose metabolism and muscle growth,[23] is responsible for improved glucose metabolism after BGN treatment. BGN successfully increased AKT phosphorylation in the absence of insulin in L6 myoblast cells (Figure 6A,B) as well as primary-cultured muscle cells (see Figure S1A), while it was reversed at 3 hours. Phosphoinositide 3-kinase (PI3K) is an upstream effector of AKT upon insulin stimulation, and inhibition of PI3K by LY-294002 attenuated

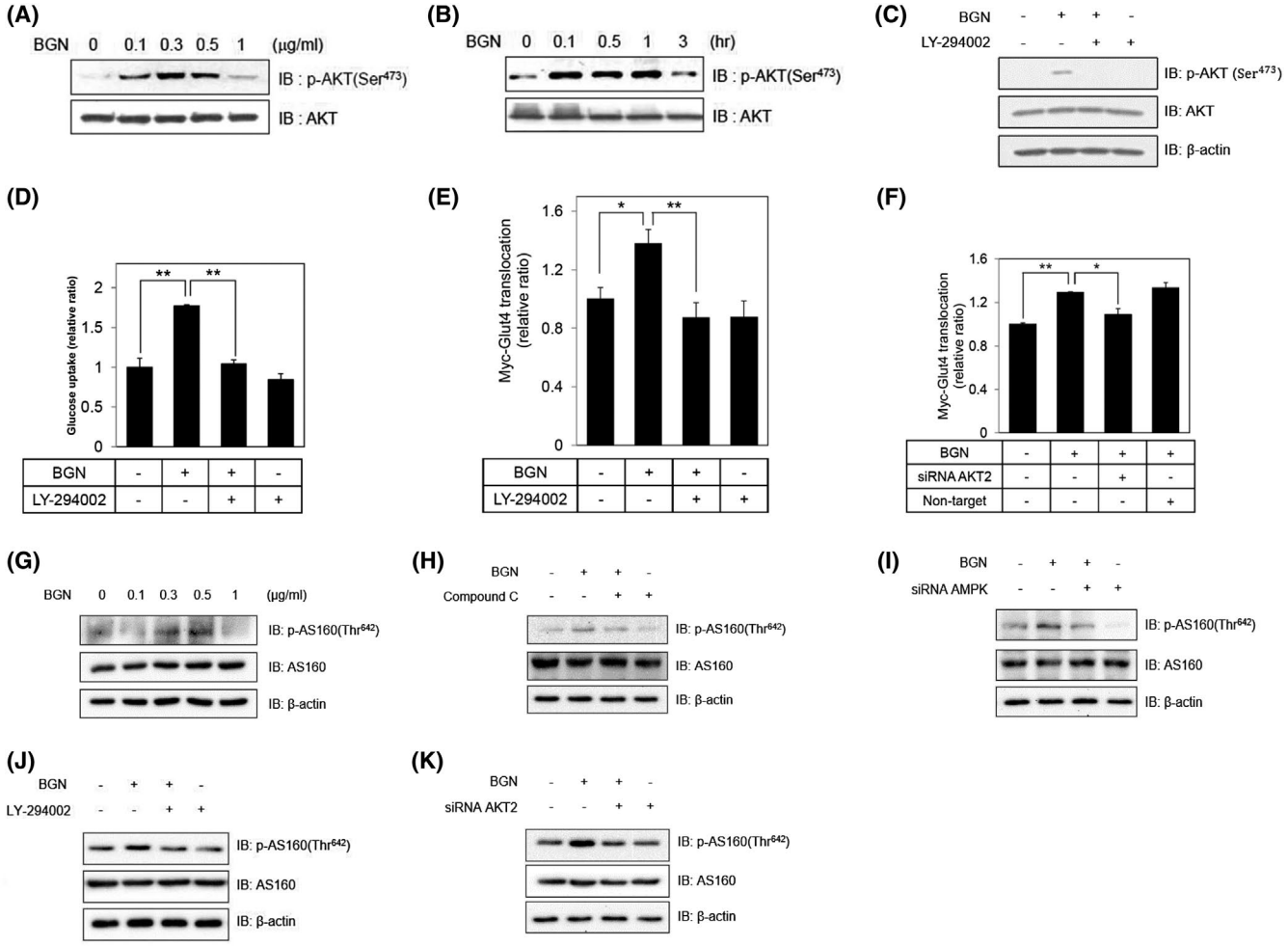

FIGURE 6 BGN induces glucose uptake via PI3K/AKT signaling-dependent AS160 activation. L6 cells were stimulated with (A) BGN (0-1 μg/mL) for 1 hour or (B) for the indicated times with a fixed dose (0.3 μg/mL) of BGN. Lysates were used for western blot against AKT and p-AKT. C, L6 cells and (D) myotubes were pre-treated with LY-294002 (PI3K inhibitor, 20 μM) and then incubated with BGN (0.3 μg/mL) for 1 hour, and western blot and glucose uptake assays were performed. E, Myotubes were treated with BGN (0.3 μg/mL) in the presence of 20 μM LY-294002. F, Myotubes lacking AKT2 were treated with BGN (0.3 μg/mL). Surface myc-GLUT4 level was quantified using an antibody-coupled colorimetric absorbance assay. Non-target antibody was used for negative control. G-K, Western blot images of AS160, p-AS160, and β-actin from L6 cells. G, Cells were treated with BGN in various concentrations for 1 hour. To confirm whether AMPK is involved in BGN-mediated AS160 phosphorylation, cells were pre-incubated with (H) 30 μM compound C or (I) transfected with AMPK-specific siRNA and stimulated with BGN (0.3 μg/mL). To test whether AKT is responsible for BGN-mediated AS160 phosphorylation, cells were pre-incubated with (J) 20 μM LY-294002 or (K) transfected with AKT2-specific siRNA and stimulated with BGN (0.3 μg/mL). * $P < .05$, ** $P < .01$. All data are expressed as mean ± SEM (n = 3)

BGN-mediated AKT activation (Figure 6C) and glucose uptake (Figure 6D). Furthermore, significantly attenuated GLUT4 translocation was observed in the presence of LY-294002 (Figure 6E) or siRNA targeting of AKT2 (Figure 6F). Overall, these results show that PI3K/AKT is the underlying molecular mechanism for the action of BGN in glucose control.

3.7 | BGN activates AS160 phosphorylation in L6 myoblast cells

AMPK and AKT have been reported to phosphorylate AS160, also known as TBC1 domain family member 4 (TBC1D4), at T642, designating GLUT4 to the plasma membrane.[24] In this study, BGN increased phosphorylation

of AS160 in L6 myoblast cells (Figure 6G). To investigate the pathway responsible for AS160 phosphorylation, we tested whether BGN treatment affects AS160 phosphorylation with inhibition of either AMPK or AKT signaling in L6 myoblast cells (Figure 6H-K). Compound C and AMPK-specific siRNA blocked BGN-mediated AS160 phosphorylation (Figure 6H,I); the same was found with LY-294002 and siRNA targeting AKT2 in L6 myoblast cells (Figure 6J,K). These findings indicate that BGN affects AS160 phosphorylation and subsequent GLUT4 translocation through AMPK/AKT dual pathways.

4 | DISCUSSION

Obesity and impairment in glucose metabolism have been established as risk factors for type 2 diabetes,[25,26] of which the age standardized prevalence worldwide has increased since 1980.[27] BGN has recently been suggested as a signaling molecule distinct from its role as an ECM component.[28] Nevertheless, the metabolic effects of BGN as a ligand have remained unknown. In this study, we observed multiple metabolic effects of BGN including regulation of energy metabolism (appetite, body weight, and muscle synthesis) and glucose metabolism. More specifically, we demonstrated that BGN effectively reduces food intake by modulating hypothalamic gene expression involved in appetite, which was associated with the prevention of body weight gain in diet-induced obese animals. In addition, we showed that BGN treatment improves glucose metabolism in vitro and in vivo.

In this study, BGN-reduced body weight gain in HFD mice was attributable to reduced food intake. Regulation of appetite is primarily mediated by the arcuate nucleus neurons that reside in the hypothalamus[29]; thus, we tested the direct effects of BGN on the expression of neuropeptides regulating food intake in both hypothalamic cell lines and the hypothalamus of animals. In hypothalamic neuronal cell lines, anorexigenic POMC and orexigenic Agrp/NPY expression were shown to be acutely modulated by BGN treatment. This was further demonstrated in mice ICV administered with BGN, showing that hypothalamic regulation on appetite genes is also active under physiological conditions. By contrast, we also found that these modulations in the expression of hypothalamic neuropeptides were reversed 24 hours after ICV injection of BGN. This may be due to a negative mechanism to compensate for the hyperactivity of BGN. In vivo, the arcuate nucleus neurons receive hormonal signals such as insulin and leptin, from the pancreas and adipose tissues, respectively, upregulating the anorexigenic neuropeptides and downregulating the orexigenic neuropeptides expressions.[30] One possible explanation might be that the insulin or leptin could be reduced by 24 hours treatment of BGN, restraining the POMC expression to restore a sustained and severely reduced supply of energy under the circumstances of negative energy balance. Although this rebounded action for energy balance happens, it is clear that BGN increases POMC and decreases Agrp/Npy gene expression in vivo and vitro. To investigate molecular mechanism underlying appetite-related gene expression by BGN, we explored whether activation of the hypothalamic AKT-FoxO1-mediated signaling pathway affects this in vitro. Phosphorylated AKT enters the nucleus and phosphorylates the transcription factor FoxO1, resulting in the modulation of appetite-related gene expression.[31] In this study, no changes in the phosphorylation of AKT and FoxO1 were at the time points where the NPY and POMC were changed by BGN treatment in N41 and N43/5. One study using transcriptome profiling reported that the signaling pathways related to oxidative phosphorylation, glucose and lipid metabolism, and neurotrophin were highly altered in the hypothalamus of *Bgn* knockout mice.[32] The data showing differentially expressed genes and pathways in the hypothalamus by *Bgn* knockout might be helpful to find candidates responsible for BGN-mediated regulation of hypothalamic neuropeptide expression for future studies. While the exact mechanism responsible for the modulation of neuropeptide expression by BGN treatment remains unclear, it is also unknown whether BGN can cross blood-brain barrier (BBB). In our data of Figures 2 and 3, IP or ICV injection of BGN decreases food intake and bodyweight. Although it is unclear whether the changes in food intake and body weight by IP injection are due to the passage of BGN to BBB, the central effect of BGN by ICV injection suggests that BGN might cross BBB through an unknown transporter and lead to changes in food intake and bodyweight. Despite the lack of information how peripherally derived BGN reaches brain to participate in its CNS actions, our results clearly showed that BGN administration elicits reductions in body weight by regulating food intake in diet-induced obese animals and in mice ICV administered with BGN (Figure 7).

Because obesity is associated with abnormalities in glucose metabolism, we next tested whether BGN influences glucose homeostasis. We observed herein that BGN successfully improved glucose metabolism in HFD-fed mice, but this should be carefully interpreted as DIO is not fully corresponding to diabetes-mediated changes in glucose metabolism. Furthermore, based on the fact that skeletal muscle contributes largely to glucose homeostasis by facilitating glucose uptake,[33] we evaluated the effect of BGN on glucose uptake and GLUT4 translocation in L6 myoblast cells. In this study, BGN effectively stimulated phosphorylation of AMPK and AKT, thereby enhancing glucose uptake and GLUT4 translocation. Indeed, AMPK and AKT are generally accepted to respond to exercise/muscle contraction and insulin/PI3K, respectively.[34-36] At a cellular level, BGN spontaneously induced intracellular Ca^{2+} release and CAMKK-dependent AMPK activation while PI3K-dependent AKT phosphorylation was

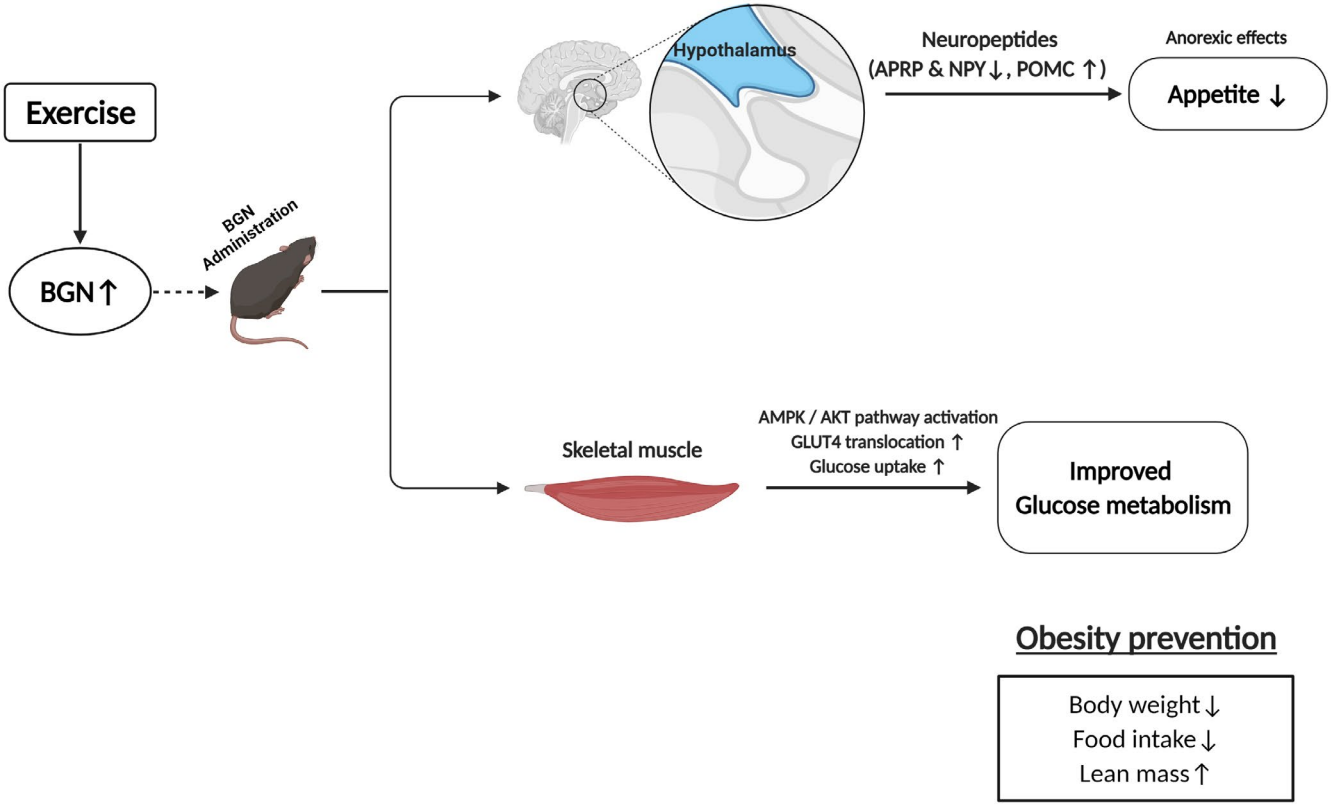

FIGURE 7 A graphical scheme illustrating the working mechanism of biglycan

also detected. Importantly, BGN-mediated glucose uptake was significantly attenuated by both AMPK and AKT inhibitors. This suggests that BGN acts through multiple pathways. Furthermore, BGN phosphorylates a known downstream effector of AMPK and AKT, AS160 (also known as TBC1D4), at T642. AMPK and AKT increase glucose uptake via phosphorylation of AS160 and promotion of GLUT4 translocation to plasma membrane.[37] In line with this, our data showed that AKT2- or AMPK-specific silencing by siRNA or inhibition by compound C or LY-294002 abolished the effects of BGN on AS160 phosphorylation and GLUT4 translocation. Taken together, our results demonstrate that BGN is effective in the improvement of glucose metabolism in skeletal muscle cells in vitro and in vivo.

We speculate that the mechanism by which BGN controls body weight and glucose metabolism is that BGN may act as a myokine regulates whole-body metabolism via autocrine or paracrine mechanisms. Indeed, *bgn* mRNA expression levels increased after electrical pulse stimulation system in a time-dependent manner in addition to an increase in AMPK phosphorylation. Also, circulating BGN levels were elevated in mice exposed to acute exercise, and AMPK phosphorylation levels were higher in these mice than in controls. This was further supported by the finding that BGN-treated HFD mice had significantly higher muscle mass than HFD mice alone, indicating its effect possibly via an autocrine function. This increased muscle mass may be partly explained by phosphorylation of AKT and mTORC1 being upregulated by BGN treatment in L6 myoblast cells (Shin MJ, unpublished data). Increased muscle mass is favorably associated with cardiometabolic phenotypes such as obesity, insulin resistance, and type 2 diabetes mellitus.[38,39] Therefore, these results collectively suggest that BGN is a myokine secreted by muscle contraction; thus, BGN treatment, as a soluble ligand, may contribute positively to metabolic processes through communication with other organs. However, BGN has been reported to be expressed in diverse tissues including adipose tissues, kidney, muscle, etc[40-45] Whether the effects observed in this study are exclusively derived by the action of BGN as a myokine requires further investigation.

Alternatively, it is also possible that BGN may act as insulin mimetic. It has been suggested that insulin stimulates AKT-FoxO1 signaling, thereby regulating Agrp/NPY and POMC in the hypothalamus.[46] Indeed, in vitro data in this study showed that BGN is involved in the regulation of appetite in hypothalamic cell lines in the absence of insulin although it was not mediated by AKT-FoxO1 signaling. In contrast, PI3K/AKT-dependent GLUT4 translocation in skeletal muscle cells was stimulated by BGN, independently of insulin. In addition, specific inhibition of the primary target of insulin, PI3K, disrupts BGN activity on glucose uptake in L6 myoblast cells. Furthermore, BGN activates the AKT phosphorylation site of AS160 (T462), which is reported to play a critical role for insulin-mediated

glucose uptake,[47] indicating the role of BGN as an insulin mimetic.

In conclusion, we report that BGN administration significantly prevented diet-induced obesity, and this was mainly accounted for by reduced food intake. BGN treatment modulated genes involved in appetite in the hypothalamus. In addition, BGN regulates glucose metabolism as shown by improved glucose tolerance in mice and enhanced glucose uptake and GLUT4 translocation in L6 myoblast cells as well as primary skeletal muscle cells. In this process, BGN improved glucose metabolism through AMPK/AKT dual pathways. Because obesity and glucose intolerance are commonly found in metabolic disturbances[48] and are highly interrelated, it will be important to elucidate whether the observed improvement in glucose metabolism by BGN treatment is independently achieved or a secondary effect of reductions in food intake and body weight. Our results suggest that BGN acts as a novel candidate for therapeutics in risk factors for metabolic diseases attributable to physical inactivity.

CONFLICT OF INTEREST

The authors have no relevant conflict of interest to disclose.

AUTHOR CONTRIBUTIONS

H.S. Kim and M.J. Shin conceived the study. E.K. Kim, H.S. Kim, and M.J. Shin designed and directed the project. I. Chung, S.A. Kim, S. Kim, J.O. Lee, C.Y. Park, J. Lee, J. Kang, J.Y. Lee, I. Seo, H.J. Lee, J.A. Han, M.J. Kang, E. Lim, S.J. Kim, S.W. Wu, and J.Y. Oh performed the experiments and acquired the data. I. Chung, S.A. Kim, E.K. Kim, H.S. Kim, and M.J. Shin analyzed and interpreted the results and prepared the manuscript. I. Chung, S.A. Kim, J.H. Chung, E.K. Kim, H.S. Kim, and M.J. Shin reviewed and edited the manuscript.

REFERENCES

1. Schaefer L, Iozzo RV. Biological functions of the small leucine-rich proteoglycans: from genetics to signal transduction. *J Biol Chem*. 2008;283:21305-21309.
2. Ameye L, Aria D, Jepsen K, Oldberg A, Xu T, Young MF. Abnormal collagen fibrils in tendons of biglycan/fibromodulin-deficient mice lead to gait impairment, ectopic ossification, and osteoarthritis. *FASEB J*. 2002;16:673-680.
3. Ameye L, Young MF. Mice deficient in small leucine-rich proteoglycans: novel in vivo models for osteoporosis, osteoarthritis, Ehlers-Danlos syndrome, muscular dystrophy, and corneal diseases. *Glycobiology*. 2002;12:107R-116R.
4. Berendsen AD, Fisher LW, Kilts TM, et al. Modulation of canonical Wnt signaling by the extracellular matrix component biglycan. *Proc Natl Acad Sci*. 2011;108:17022-17027.
5. Schaefer L, Babelova A, Kiss E, et al. The matrix component biglycan is proinflammatory and signals through Toll-like receptors 4 and 2 in macrophages. *J Clin Investig*. 2005;115:2223-2233.
6. Babelova A, Moreth K, Tsalastra-Greul W, et al. Biglycan, a danger signal that activates the NLRP3 inflammasome via toll-like and P2X receptors. *J Biol Chem*. 2009;284:24035-24048.
7. Parisuthiman D, Mochida Y, Duarte WR, Yamauchi M. Biglycan modulates osteoblast differentiation and matrix mineralization. *J Bone Miner Res*. 2005;20:1878-1886.
8. Amenta AR, Yilmaz A, Bogdanovich S, et al. Biglycan recruits utrophin to the sarcolemma and counters dystrophic pathology in mdx mice. *Proc Natl Acad Sci*. 2011;108:762-767.
9. Kang L, Ayala JE, Lee-Young RS, et al. Diet-induced muscle insulin resistance is associated with extracellular matrix remodeling and interaction with integrin α2β1 in mice. *Diabetes*. 2011;60:416-426.
10. Tervaert TWC, Mooyaart AL, Amann K, et al. Pathologic classification of diabetic nephropathy. *J Am Soc Nephrol*. 2010;21:556-563.
11. Levental KR, Yu H, Kass L, et al. Matrix crosslinking forces tumor progression by enhancing integrin signaling. *Cell*. 2009;139:891-906.
12. Huang G, Greenspan DS. ECM roles in the function of metabolic tissues. *Trends Endocrinol Metab*. 2012;23:16-22.
13. Kang L, Lantier L, Kennedy A, et al. Hyaluronan accumulates with high-fat feeding and contributes to insulin resistance. *Diabetes*. 2013;62:1888-1896.
14. Chanmee T, Ontong P, Izumikawa T, et al. Hyaluronan production regulates metabolic and cancer stem-like properties of breast cancer cells via hexosamine biosynthetic pathway-coupled HIF-1 signaling. *J Biol Chem*. 2016;291:24105-24120.
15. Ojima K, Oe M, Nakajima I, et al. Proteomic analysis of secreted proteins from skeletal muscle cells during differentiation. *EuPA Open Proteom*. 2014;5:1-9.
16. Richter EA, Ruderman NB. AMPK and the biochemistry of exercise: implications for human health and disease. *Biochem J*. 2009;418:261-275.
17. Carter S, Solomon TP. In vitro experimental models for examining the skeletal muscle cell biology of exercise: the possibilities, challenges and future developments. *Pflügers Arch Eur J Phys*. 2019;471:413-429.
18. Jeon Y, Aja S, Ronnett GV, Kim E-K. D-chiro-inositol glycan reduces food intake by regulating hypothalamic neuropeptide expression via AKT-FoxO1 pathway. *Biochem Biophys Res Commun*. 2016;470:818-823.
19. Ibrahim N, Bosch MA, Smart JL, et al. Hypothalamic proopiomelanocortin neurons are glucose responsive and express KATP channels. *Endocrinology*. 2003;144:1331-1340.
20. Bowe MA, Mendis DB, Fallon JR. The small leucine-rich repeat proteoglycan biglycan binds to α-dystroglycan and is upregulated in dystrophic muscle. *J Cell Biol*. 2000;148:801-810.
21. Lin S-C, Hardie DG. AMPK: sensing glucose as well as cellular energy status. *Cell Metab*. 2018;27:299-313.
22. Hawley SA, Pan DA, Mustard KJ, et al. Calmodulin-dependent protein kinase kinase-β is an alternative upstream kinase for AMP-activated protein kinase. *Cell Metab*. 2005;2:9-19.
23. Schiaffino S, Dyar KA, Ciciliot S, Blaauw B, Sandri M. Mechanisms regulating skeletal muscle growth and atrophy. *FEBS J*. 2013;280:4294-4314.
24. O'Neill HM. AMPK and exercise: glucose uptake and insulin sensitivity. *Diabetes Metab J*. 2013;37:1-21.
25. Chan JM, Rimm EB, Colditz GA, Stampfer MJ, Willett WC. Obesity, fat distribution, and weight gain as risk factors for clinical diabetes in men. *Diabetes Care*. 1994;17:961-969.

26. Shah M, Vella A. What is type 2 diabetes? *Medicine*. 2014;42:687-691.
27. Kwak S-Y, Chung I, Kang J, et al. Sex specific effect of ATPase inhibitory factor 1 on body weight: studies in high fat diet induced obese mice and genetic association studies in humans. *Metabolism*. 2020;105:154171.
28. Moreth K, Brodbeck R, Babelova A, et al. The proteoglycan biglycan regulates expression of the B cell chemoattractant CXCL13 and aggravates murine lupus nephritis. *J Clin Investig*. 2010;120:4251-4272.
29. Yeo GS, Heisler LK. Unraveling the brain regulation of appetite: lessons from genetics. *Nat Neurosci*. 2012;15:1343-1349.
30. Coll AP, Farooqi IS, O'Rahilly S. The hormonal control of food intake. *Cell*. 2007;129:251-262.
31. Kim M-S, Pak YK, Jang P-G, et al. Role of hypothalamic Foxo1 in the regulation of food intake and energy homeostasis. *Nat Neurosci*. 2006;9:901-906.
32. Ying Z, Byun HR, Meng Q, et al. Biglycan gene connects metabolic dysfunction with brain disorder. *Biochim Biophys Acta Mol Basis Dis*. 2018;1864:3679-3687.
33. Richter EA, Hargreaves M. Exercise, GLUT4, and skeletal muscle glucose uptake. *Physiol Rev*. 2013;93(3):993-1017.
34. Wojtaszewski JF, Nielsen P, Hansen BF, Richter EA, Kiens B. Isoform-specific and exercise intensity-dependent activation of 5′-AMP-activated protein kinase in human skeletal muscle. *J Physiol*. 2000;528:221-226.
35. Hayashi T, Hirshman MF, Kurth EJ, Winder WW, Goodyear LJ. Evidence for 5′ AMP-activated protein kinase mediation of the effect of muscle contraction on glucose transport. *Diabetes*. 1998;47:1369-1373.
36. Huang X, Liu G, Guo J, Su Z. The PI3K/AKT pathway in obesity and type 2 diabetes. *Int J Biol Sci*. 2018;14:1483.
37. Chavez JA, Roach WG, Keller SR, Lane WS, Lienhard GE. Inhibition of GLUT4 translocation by Tbc1d1, a Rab GTPase-activating protein abundant in skeletal muscle, is partially relieved by AMP-activated protein kinase activation. *J Biol Chem*. 2008;283:9187-9195.
38. Srikanthan P, Karlamangla AS. Relative muscle mass is inversely associated with insulin resistance and prediabetes. Findings from the third National Health and Nutrition Examination Survey. *J Clin Endocrinol Metab*. 2011;96:2898-2903.
39. Park SW, Goodpaster BH, Strotmeyer ES, et al. Decreased muscle strength and quality in older adults with type 2 diabetes: the health, aging, and body composition study. *Diabetes*. 2006;55:1813-1818.
40. Kim J, Lee SK, Shin J-M, et al. Enhanced biglycan gene expression in the adipose tissues of obese women and its association with obesity-related genes and metabolic parameters. *Sci Rep*. 2016;6:1-11.
41. Bianco P, Fisher LW, Young MF, Termine JD, Robey PG. Expression and localization of the two small proteoglycans biglycan and decorin in developing human skeletal and non-skeletal tissues. *J Histochem Cytochem*. 1990;38:1549-1563.
42. Högemann B, Edel G, Schwarz K, Krech R, Kresse H. Expression of biglycan, decorin and proteoglycan-100/CSF-1 in normal and fibrotic human liver. *Pathol Res Pract*. 1997;193:747-751.
43. Matsuura T, Duarte WR, Cheng H, Uzawa K, Yamauchi M. Differential expression of decorin and biglycan genes during mouse tooth development. *Matrix Biol*. 2001;20:367-373.
44. Roughley PJ, Melching LI, Recklies AD. Changes in the expression of decorin and biglycan in human articular cartilage with age and regulation by TGF-β. *Matrix Biol*. 1994;14:51-59.
45. Fisher LW, Termine J, Dejter S, et al. Proteoglycans of developing bone. *J Biol Chem*. 1983;258:6588-6594.
46. Varela L, Horvath TL. Leptin and insulin pathways in POMC and AgRP neurons that modulate energy balance and glucose homeostasis. *EMBO Rep*. 2012;13:1079-1086.
47. Kramer HF, Witczak CA, Fujii N, et al. Distinct signals regulate AS160 phosphorylation in response to insulin, AICAR, and contraction in mouse skeletal muscle. *Diabetes*. 2006;55:2067-2076.
48. Eriksson H, Welin L, Wilhelmsen L, et al. Metabolic disturbances in hypertension: results from the population study 'men born in 1913'. *J Intern Med*. 1992;232:389-395.

SUPPORTING INFORMATION

Additional Supporting Information may be found online in the Supporting Information section.

How to cite this article: Chung I, Kim SA, Kim S, et al. Biglycan reduces body weight by regulating food intake in mice and improves glucose metabolism through AMPK/AKT dual pathways in skeletal muscle. *FASEB J*. 2021;35:e21794. https://doi.org/10.1096/fj.202002039RR